

MS-DINO: Efficient Distributed Training of Vision Transformer Foundation Model in Medical Domain through Masked Sampling

Sangjoon Park^a, Ik-Jae Lee^b, Jun Won Kim^{b,*}, Jong Chul Ye^{c, **}

^a*Department of Bio and Brain Engineering, Korea Advanced Institute of Science and Technology (KAIST), Daejeon, South Korea*

^b*Department of Radiation Oncology, Gangnam Severance Hospital, Seoul, South Korea*

^c*Kim Jaechul Graduate School of AI, Korea Advanced Institute of Science and Technology (KAIST), Daejeon, South Korea*

ARTICLE INFO

2000 MSC: 41A05, 41A10, 65D05, 65D17

Keywords: Distributed learning, Self-supervised learning, Vision Transformer, Random permutation, Computed Tomography, Chest X-ray

ABSTRACT

In spite of the recent success of deep learning in the medical domain, the problem of data scarcity in the medical domain gets aggravated due to privacy and data ownership issues. Distributed learning approaches including federated learning have been studied to alleviate the problems, but they suffer from cumbersome communication overheads and weakness in privacy protection. To address this, here we propose a self-supervised masked sampling distillation method for vision transformer that can be performed without continuous communication but still enhance privacy using a vision transformer-specific encryption method. The effectiveness of our method is demonstrated with extensive experiments on two medical domain data and two different downstream tasks, showing superior performances than those obtained with the existing distributed learning strategy as well as the fine-tuning only baseline. As the self-supervised model built with the proposed method is capable of having a general semantic understanding of the modality, we demonstrate its potential as a task-agnostic foundation model for various medical tasks, widening the applicability in the medical domain.

© 2023

1. Introduction

The success of deep learning (DL) has made it de facto standard in developing artificial intelligence (AI) powered medical tools (Lee et al., 2017; Ting et al., 2018; Giger, 2018; Pesapane et al., 2018), but the data and label-driven nature of the deep learning requires imperative collaboration between multiple institutions. However, strict legal or institutional regulations often forbid the free sharing of data derived from patients due to privacy concerns (Edemekong et al., 2018; Hoofnagle et al., 2019). Usually, the de-identified data can be shared only between the collaborators under formal consents, which can be one of the most cumbersome obstacles in AI research. Distributed learning methods like federated learning (FL) (Konečný et al., 2016) and split learning (SL) (Vepakomma et al., 2018) have been introduced to cope with this problem by alleviating the data governance and ownership issues.

In the FL, the goal is to obtain a model on the server-side while training data remain unmoved over the edge devices of

multiple clients. In detail, the central server distributes the global model to each client, and the clients perform training iterations with their data in parallel, to return the results of local computations to the server. The server then aggregates and averages local updates, and distributes again the updated global model. This process is repeatedly performed until the model converges. While the FL has resolved the issues of data sharing, it does not fully guarantee privacy. Specifically, data can leak by reconstructing the private data used in training with the inversion attack which uses the stolen gradients of local model updates from insecure aggregation (Geiping et al., 2020). In addition, it imposes heavy computational loads on the edge devices of the clients as the most of computations and updates of the model are performed in client-side devices (Li et al., 2020b; Mammen, 2021).

In the SL, on the other hand, the entire model is split into several sub-networks trained separately on the server-side and client-side. Specifically, the first sub-network performs a forward pass on the client-side device and sends the smashed features to the second sub-network located on the server-side. The server then performs forward propagation with these features to pass back the subsequent features to the third sub-network on the client side. The third sub-network on the client side can

*Co-corresponding author: Tel.: +82-2-2019-3152; fax: +82-2-2019-4855;

**Co-corresponding author: Tel.: +82-42-350-4320; fax: +82-42-350-4310;

e-mail: junwon@yuhs.ac, jong.ye@kaist.ac.kr (Jong Chul Ye)

yield the outcome of the model, and the loss can be calculated with the client-side label. Backpropagation through split sub-networks on clients and server-sides is performed in the exact opposite manner to the forward pass. Allocating small-sized sub-networks to train on the client-side device reduces the computational load of local clients that usually lack resources in practical implementation. In addition, the SL offers model privacy by inserting black-box to clients and server, preventing both from having access to the full network. However, there remain privacy concerns like the hijacking of transmitted features to be inverted to the original data (Gawron and Stubbings, 2022).

Besides these limitations, these methods may impose substantial communication overheads in practical implementation. For instance, FL requires the entire model, which is usually large-sized, to be aggregated and distributed between the server and clients. Meanwhile, the feature and gradients from the split subnetwork should be continuously interchanged in a relay-based manner in the SL, enforcing the clients to be connected during the entire training process (Li *et al.*, 2020b).

Recently, a pure attention-based DL model named Vision Transformer (ViT) (Dosovitskiy *et al.*, 2020) has been introduced to the vision community and has become a core component of vision research. The ViT has several desirable properties thanks to its simple but powerful attention architecture, and recent efforts to understand the properties of the ViT have found that it has more shape-biased nature like human and is less susceptible to perturbation like occlusion or random patch permutation (Naseer *et al.*, 2021). In addition, several recent works on self-supervised learning have reported that the ViT-based model can benefit more from the various self-supervised learning schemes like learning semantic meaning with knowledge distillation (Caron *et al.*, 2021) or masked patch prediction (Bao *et al.*, 2021; He *et al.*, 2022).

Inspired by the properties of ViT, here we present a novel distributed self-supervised learning strategy to build a foundation model that does not require continuous communication between server and clients. In detail, our insight comes from the permutation invariant properties of self-attention can be utilized to offer the encryption by *feature-space random permutation* (Park and Ye, 2022). On top of this, we exploit another important property of ViT resulting from its patch-based image processing, which enables the random masked sampling-based self-supervised learning to train the foundation model solely on the server-side, eliminating the need for continuous communication.

Our contributions can be highlighted as follows:

- We tackle the cumbersome problems of distributed self-supervised learning by introducing a novel method that effectively leverages the properties of ViT.
- We conduct extensive experiments to show the superiority of the proposed method on two medical domain data and tasks, i.e., organ-at-risk (OAR) segmentation in computed tomography (CT) and tuberculosis diagnosis in chest X-ray (CXR).
- We experimentally prove the infeasibility of a privacy at-

tack on the proposed methods, implying that the proposed method can offer better privacy compared with the existing approaches.

2. Related Works

2.1. Self-supervised Vision Transformer

Self-supervised learning is gaining traction in the vision community due to its outstanding successes in recent years, reducing the gap with supervised learning (Jing and Tian, 2020; Liu *et al.*, 2021). A line of works on self-supervised learning leverages an approach to train the model by discriminating the differently augmented versions of the given image, commonly called contrastive learning (Jaiswal *et al.*, 2020). In a pioneering work, Caron *et al.* (2021) proposed a contrastive learning method that allows the ViT to use contrastive learning via teacher-student knowledge distillation, called distillation without a label (DINO), eliminating the need for cumbersome negative samples required in traditional contrastive learning methods (Chen *et al.*, 2020b; Grill *et al.*, 2020; Zbontar *et al.*, 2021). In this method, the model learns the task-agnostic semantic meaning of the image through local-to-global correspondence with a random multi-crop strategy. When visualizing the self-attention of the ViT model with DINO, the instance-level visual semantics were well attended by the model, without any supervision for instance segmentation. This property was only observable in ViT, and better performances in both linear probes and fine-tuning were observed in ViT compared to the CNN-based model.

Since the ViT model is designed to be a pure patch-based attention model, another strong self-supervised learning technique, random masked patch prediction, can be utilized for ViT-based models, which resembles the masked language modeling for Bidirectional Encoder Representations from Transformers (BERT) pre-training in the field of natural language processing (NLP) (Devlin *et al.*, 2018). Bao *et al.* (2021) proposed a Bidirectional Encoder representation from Image Transformers (BEiT) that learns to predict the masked patch with discrete visual tokens obtained with the discrete tokenizer, demonstrating that the same strategy in BERT can also be leveraged in vision tasks. Instead of predicting discrete tokens, He *et al.* (2022) proposed a rather simple strategy of learning directly from predicting pixels within the masked patches called masked autoencoder (MAE), by adopting computation efficient encoder-decoder design. These random masking-based learning strategies are specially designed for the ViT that process the image in a patch-wise manner and are not suitable for a CNN-based model that leverages the shared convolution kernels stride across the image.

2.2. Federated Split Task-Agnostic Learning with Permutating Pure ViT (*p*-FeSTA)

Inspired by the modular configuration of the ViT model that can be divided into the embedder head, transformer body, and task-specific tail (Chen *et al.*, 2020a), the *Federated Split Task-agnostic* (FeSTA) learning has been proposed to maximally exploit the distinct strengths of the FL and SL methods (Park

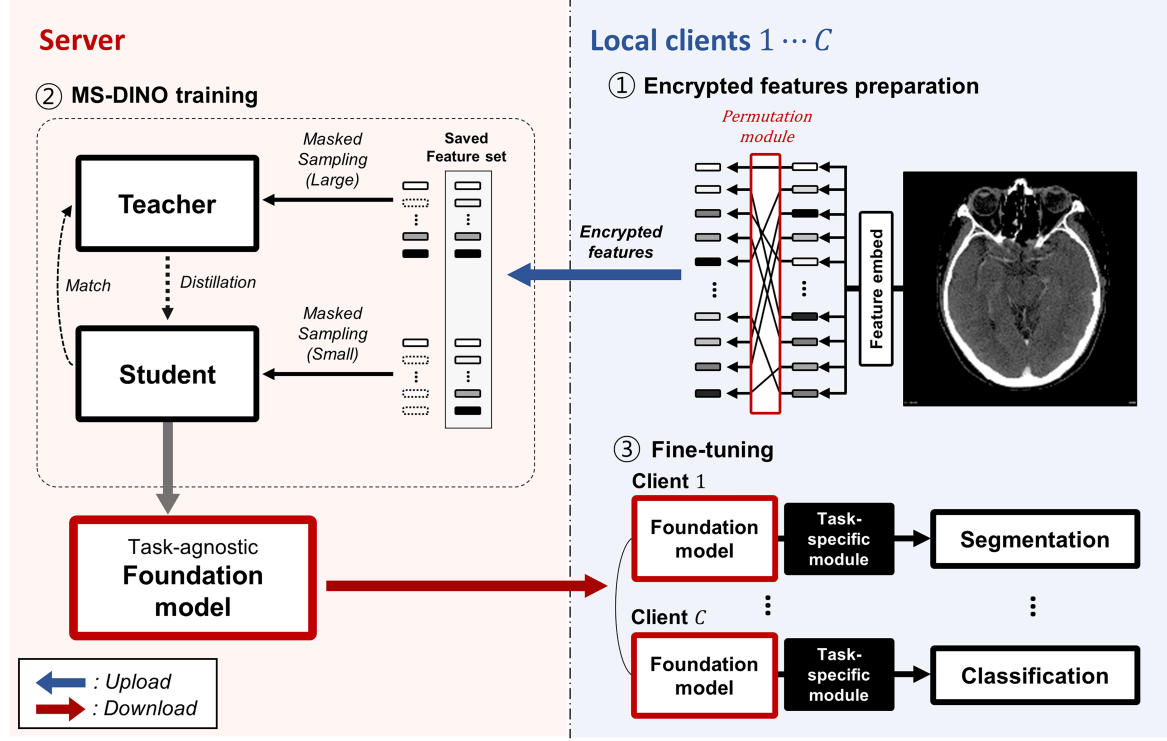


Fig. 1. Overall framework. First, the participating clients transmit the patch features encrypted with the arbitrary patch embedder and the *feature-space permutation module* to the server. Then, the MS-DINO training is performed on a server-side device to make the foundation model to have a general semantic understanding of the modality. Finally, the trained foundation model can be accessed by authorized clients to be used for various downstream tasks.

et al., 2021), and to improve the performances of the individual tasks with the collaboration between the participating clients with different tasks. In more recent work, *Federated Split Task-Agnostic Learning with Permutating Pure ViT* (*p*-FESTA) has been introduced to surmount the drawbacks of the FESTA (Park and Ye, 2022) by leveraging the permutation-invariant property of the ViT by adopting random patch permutation to provide better privacy as well as fewer communication overheads. The main motivation of the *p*-FESTA method is to reduce the communication between the server and clients as well as enhance the privacy with the permutation module in the feature space, which is possible via the permutation invariant property of the transformer encoder layers, the main component of ViT. Specifically, the model can be trained with the patch features permuted in the feature space with the novel *feature-space permutation module*, which provides privacy by keeping the malicious attackers from faithfully reconstructing the private data from the intermediate features. These permuted features can be safely saved in the server-side memory and used throughout the entire learning process, easing the burden to approximately half of the FESTA. However, this method is also not free of limitations that restrict the generalized application. First, continuous communication between the server and clients is mandatory for model training as the labels are required for the update of the shared transformer body. Second, multi-task learning was possible only with the clients simultaneously participating in distributed learning who want to perform relevant tasks.

3. Proposed Framework

The proposed self-supervised learning method, dubbed *Masked Sampling Distillation with No Label* (MS-DINO), is composed of three steps. First, the patch features from all images were extracted by an arbitrary patch embedder along with another arbitrary position embedding, and their sequence is randomly permuted with *feature-space permutation module*. Then, the encrypted patch features are transmitted to the server and stored. The server-side computational device uses these encrypted features throughout the entire learning process of the foundation model with no further communication with the clients. Finally, the trained foundation model can be accessed by the authorized clients for the application of downstream tasks, offering performance superior to the fine-tuning-only baselines. The overall framework is proposed in Fig. 1.

3.1. Foundation model learning

Fig. 2 illustrates the foundation model learning process with the MS-DINO method. Similar to the approach proposed in the *p*-FESTA, given the image data of client x , the intermediate patch features f are extracted from the arbitrary patch feature extractor F , and permuted with the *feature-space permutation module* permute , which can be defined as $f = \text{permute}(F(x))$. Then, the encrypted features are transmitted from each client c to the server. This process is performed at the beginning of the learning process, and the remaining processes are performed solely on the server-side, eliminating the need for both further

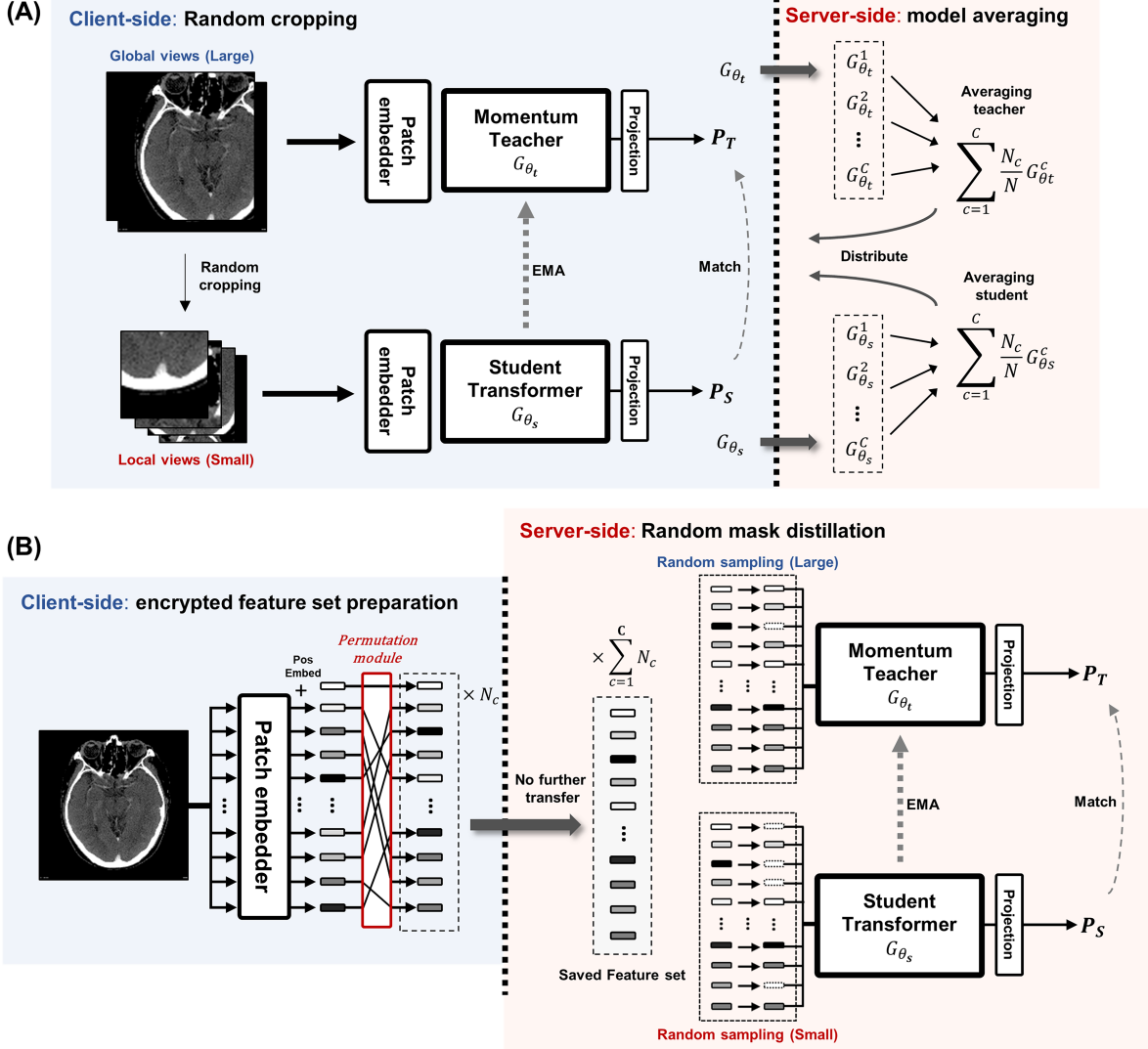


Fig. 2. Comparison of (A) the Distillation with No Labels (DINO) trained with federated learning (FL) and (B) the Masked Sampling Distillation with No Labels (MS-DINO). Compared with the original DINO method where the model gets general semantic understanding via local-to-global correspondence between the student and the momentum teacher, the model learns smaller number-to-larger number correspondence between the student and the momentum teacher in the MS-DINO method, enabling the training with randomly permuted patch features.

communication and computation overheads in client-sides. In the process of the feature extraction and encryption, we not only extracted features from the original image x but also from another randomly augmented version of the image \hat{x} to provide diversity in data, resulting in two different encrypted features data per image as below.

$$f = \text{permute}(F(x)), \quad \hat{f} = \text{permute}(F(\hat{x})) \quad (1)$$

As the features are encrypted with both the patch embedder unknown to the server along with the unknown position embed and the permutation module in the feature space, it is infeasible for the server to faithfully reconstruct the private data with the transmitted feature. The detailed formulation and experiments of the privacy protection will be discussed in Section 3.3 and 6.5.

With the encrypted features from all participating clients, the server performs random masked sampling-based self-supervised learning, by substituting the local-to-global of the original DINO correspondence learning strategy with small-to-large patches correspondence (Fig. 2). As illustrated in Fig. 2(A), the motivation of DINO is to teach the model the visual semantics of the image with the teacher-student knowledge distillation, by providing the *global views* with larger crops to the teacher and the multiple *local views* with smaller crops to the student. We adopted and modified this key concept into random masked sampling, by substituting the *global views* as the larger number and the *local views* as the smaller number of patch features sampled as illustrated in Fig. 2(B). In detail, for the permuted feature f obtained from an image, the majority of the permuted patch features are randomly sampled to make the feature f_l , and a relatively smaller number of the patches are randomly sampled resulting in the feature f_s . Like DINO, f_l is

fed to the teacher, while both f_l and f_s are fed to the student. Then, the student is optimized to match the prediction of the momentum teacher with relatively small information about the image, in line with the local-to-global correspondence strategy of the DINO.

Supposing the original feature f_o , large sampled feature f_l , small sampled features f_s , the set that contains f_o , f_l , and N differently sampled f_s can be defined as $V = \{f_o, f_l, f_s^1, \dots, f_s^N\}$. Given the teacher and student models as G_{θ_t} and G_{θ_s} , the cross-entropy loss as \mathcal{L} , the student is trained to mimic the teacher's prediction with following optimization problem:

$$\min_{G_{\theta_s}} \sum_{f \in \{f_o, f_l\}} \sum_{\substack{f' \in V \\ f' \neq f}} \mathcal{L}(G_{\theta_s}(f'), G_{\theta_t}(f)) \quad (2)$$

During the learning process, the momentum teacher model is updated with an exponential moving average (EMA) of the student's update, where λ follows a cosine scheduling:

$$G_{\theta_t} = \lambda G_{\theta_t} + (1 - \lambda) G_{\theta_s} \quad (3)$$

The algorithm for the encrypted feature set preparation and the foundation model learning with MS-DINO are formally presented in the algorithm 1.

Given the limited data availability for a single client, this foundation model may merit improved generalization performance, which is further investigated in Section 6.2 and 6.3.

3.2. Fine-tuning for Tasks of Interest

As depicted in Fig. 1, the authorized clients can access the trained foundation model for their purposes. For instance, if clients seek to train an OAR segmentation model for radiotherapy planning, they can leverage the foundation model to enhance the generalization performance, since it holds the general ability to attend to visual semantics within the image.

Specifically, for client, c , supposing the pre-trained foundation model backbone as G and task-specific layer like decoder as H_c , data and label for fine-tuning as x_c and y_c , task-specific loss function as \mathcal{L}_c , the following optimization problem is solved for the fine-tuning:

$$\min_{G, H} \sum_{i=1} \mathcal{L}_c(H_c(G(x_c)), y_c) \quad (4)$$

3.3. Protecting Privacy with Feature-space Permutation Module

Protecting privacy by randomly permuting patch features in the feature space has been investigated in the previous work (Park and Ye, 2022). As the embedded features from the clients are saved on the server-side, privacy concerns may arise if the “honest-but-curious” server or the malicious attacker who has hijacked the features during the transmission may try to revert the features into the original data.

Specifically, suppose that the encrypted features with permutation are hijacked during the communication and there are sufficient public data in the same domain available for the attacker. Then, the attacker needs to solve two problems simultaneously: (1) training the attacker-side feature extract that can embed the

Algorithm 1 Proposed MS-DINO algorithm

```

/* Run on Client  $c$  */
1 Function ClientMain:
2   Client initialize with arbitrary feature embedder  $F$ 
3   for data  $x \in \{1, 2, \dots, X\}$ 
4      $\{x, x'\} \leftarrow \text{Augment}(x)$ 
5      $f = \text{permute}(F(x))$  // original feature
6      $f' = \text{permute}(F(x'))$  // augmented feature
7     feature set  $\mathbf{f} = \{\{f_1, f'_1\}, \{f_2, f'_2\}, \dots, \{f_X, f'_X\}\} \leftarrow \{f, f'\}$ 
8   return  $\mathbf{f}$ 

/* Run on Main Server */
9 Function ServerMain:
10  Server initializes student  $G_{\theta_s}$  and teacher  $G_{\theta_t}$ 
11  for clients  $c \in \{1, 2, \dots, C\}$  do in parallel
12     $\mathbf{f}_c \leftarrow \text{ClientMain}(c)$ 
13    Memory =  $\{\mathbf{f}_1, \mathbf{f}_2, \dots, \mathbf{f}_c\} \leftarrow \mathbf{f}_c$ 
14    // Save all features  $\mathbf{f}_c$  in Memory

15  for epoch  $e \in \text{Memory}$ 
16    for features  $f, f' \in \{1, 2, \dots, E\}$ 
17      // Run MS-DINO learning in server-side device
18       $\mathcal{L}_{DINO} = \sum_{f \in \{f_o, f_l\}} \sum_{\substack{f' \in V \\ f' \neq f}} \mathcal{L}(G_{\theta_s}(f'), G_{\theta_t}(f))$ 
19       $\theta_s \leftarrow \theta_s - \frac{\eta}{N} \frac{\partial \mathcal{L}_{DINO}}{\partial \theta_s}$  // update student model
20       $\theta_t = \lambda \theta_t + (1 - \lambda) \theta_s$  // EMA update of teacher model

21  for clients  $c \in \{1, 2, \dots, C\}$  do in parallel
22    Distribute  $G_{\theta_s}$  to authorized client
23    // Distribute foundation model to clients

```

image into the feature space the same as that of the unpermuted hijacked feature, and (2) training the jigsaw solver to unpermute the encrypted features into unpermuted ones in the feature space of hijacked features, not in the image space.

More specifically, we denote the permuted and the original features embedded by the attacker-side model \hat{F} as \tilde{f}_{pub} and f_{pub} , respectively, the number of attacker-side images (e.g. publicly available CT or CXR images) and the hijacked encrypted features as m , and the permuted features hijacked by the attacker during communication as \tilde{f}_{priv} which is embedded by an arbitrary client-side feature embedder F .

Then, the attacker-side model \hat{F} , discriminator D , and the decoder G can be trained by optimizing the following two learning objectives:

$$\min_{\hat{F}} \max_D \sum_{i=1}^m \sum_{j=1}^n [\log(1 - D(J(\tilde{f}_{priv}^{(i)}))) + \log D(J(\tilde{f}_{pub}^{(j)}))] \quad (5)$$

$$\min_G \sum_{i=1}^m L_{decoder}(G(J(\tilde{f}_{pub}^{(i)})), x_{pub}^{(i)}) \quad (6)$$

where $L_{decoder}$ denotes reconstruction loss for decoder. Meanwhile, the second optimization problem for the jigsaw solve J

Table 1. Data for foundation model learning

Modality	Client #1	Client #2	Client #3	Client #4
CT	7,993	8,063	8,182	7,973
CXR	8,422	8,424	8,422	8,422

can be formulated as follow:

$$\min_J \sum_{i=1}^m L_{jigsaw}(J(\tilde{f}_{pub}^{(i)}, f_{pub}^{(i)})) \quad (7)$$

where L_{jigsaw} denotes similarity loss in the feature space.

Note that to simultaneously solve the first two equations, Eq. (5) and Eq. (6), the exact jigsaw solver should be unraveled, which can be obtained if the Eq. (7) is successfully solved. However, the jigsaw solver should be trained and utilized in the same feature space as the hijacked encrypted feature, which necessitates knowing the correct solution for the attacker model \hat{F} to embed the same feature space, and this is conversely the target of the optimization problem Eq. (5). Combined, optimization of Eq. (5), Eq. (6), and Eq. (7) requires to already have each other's solutions, indicating that the problems are underdetermined and practically hard to solve.

Section 6.5 provides experimental results to support our assertion.

4. Datasets

We investigated the applicability of the proposed method in two different domain data and two different tasks, OAR segmentation with CT for radiotherapy planning and tuberculosis diagnosis with CXR.

4.1. Datasets for foundation model learning

For the foundation model learning, two open-sourced datasets, CT scans of the head and neck cancer patients from The Cancer Imaging Archive (TCIA) Head and Neck Squamous Cell Cancer (HNSCC) data (Grossberg A *et al.*, 2020; Grossberg *et al.*, 2018; Elhalawani *et al.*, 2017; Clark *et al.*, 2013) and the CXR images from the Radiological Society of North America (RSNA) pneumonia detection challenge data (of North America, 2018) were used.

To simulate the application in clinical collaboration, we simulated the collaboration of four clients with different data divisions, emulating the collaboration between four institutions. We divided the dataset into several subsets, defining each subset as the data of each client as shown in Table 1. Among the CT scans of a total of 619 patients from the HNSCC data, we used the CT scans of 200 patients, 7,993 CT slices from 50 patients (client #1), 8,063 from 50 patients (client #2), 8,182 from 50 patients (client #3) and 7,973 from 50 patients (client #4) were assigned for each client. Similarly, among a total of 33,690 images from the RSNA pneumonia detection challenge dataset, 8,422 (client #1), 8,424 (client #2), 8,422 (client #3), and 8,422 (client #4) images were assigned for each client (Table 1).

Table 2. Data for fine-tuning downstream task

Task	Description	Fine-tune		Test
		Full	Limited	
CT segmentation	OARs	2,911	608	521
	Normal	4,127	327	92
CXR classification	Tuberculosis	1,135	335	46

4.2. Datasets for fine-tuning downstream task

In practical implementation, the trained foundation model will be accessed and fine-tuned for the client's task of interest. Therefore, we used the datasets containing both data and labels for the downstream tasks, namely OAR segmentation with CT and tuberculosis diagnosis with CXR. Given the problem of limited data and label availability frequently with a single client, we performed the experiments in two settings: data-abundant (full) and data-insufficient (limited) settings.

For the downstream OAR segmentation task with CT, the Medical Image Computing and Computer Assisted Intervention (MICCAI) 2015 head and neck challenge dataset (Computing and Interventions, 2015) was used as the fine-tuning dataset for organ-at-risk segmentation. As the dataset contains a total of 2,911 CT slices and labels from 38 patients, all patients' data were utilized for the data-abundant setting, while the 8 patients' data containing 608 CT slices were used as the data-insufficient setting. For the downstream tuberculosis diagnosis task with CXR, 1,135 tuberculosis and 4,127 normal cases from two data sources, the Montgomery County (MC) dataset (Jaeger *et al.*, 2014) and TBX 11K dataset (Liu *et al.*, 2020) were collected for data-abundant setting. For data-insufficient setting, only the MC dataset containing 335 tuberculosis and 327 normal cases was used (Table 2).

4.3. Datasets for evaluation

To evaluate the benefit of the foundation model, we used two datasets for each task. For evaluation of the segmentation performance, we used the CT and region-of-interest (ROI) data collected and delineated by the board-certified radiation oncologists from the local institution (Gangnam Severance Hospital) to externally validate the performance of the developed model. From 2007 to 2021, data from 44 head and neck cancer patients were collected, and seven patient data containing all ROIs were used for the evaluation. For evaluation of the classification performance, we used a publicly accessible dataset (India tuberculosis dataset) (radder), which can be regarded as the external validation that is collected from the data source different from the training and fine-tuning.

5. Implementation Details

5.1. Details of Model development

The CT images underwent preprocessing by cropping the center area of 224×224 from a total size of 512×512 . The upper and lower window of the Hounsfield unit (HU) were set to -200 and 200, respectively, in consideration of the ranges

of HU of the OARs of interest. As the data were from different sources, the pixel spacing was adjusted to match between datasets. The CXR images were preprocessed with histogram equalization Gaussian blurring and normalization, and finally resized to 224×224 .

As the arbitrary feature embedder, the patch embedder of the DINO model pre-trained on ImageNet was used. The embedded features were permuted with the *feature-space permutation module* proposed in Park and Ye (2022), yielding the encrypted features for foundation model learning. For the body part of the Transformer, the transformer encoder of ViT small having 6 heads, 12 layers, and a patch size of 8 was used, which was initialized with the DINO self-supervised learning weights on the ImageNet.

We used the same-sized teacher and student models, and the multi-masked sampling strategy was adopted instead of the multi-cropping strategy following the original implementation of Caron *et al.* (2021). As a global view, the smaller number of patch features were masked, resulting in the ratio of 0.9 - 1.0 and 0.8 - 1.0 being sampled for CT and CXR, respectively. For multiple local views, the larger number of patch features were masked, sampling with a ratio of 0.3 - 0.5 and 0.3 - 0.4 for CT and CXR. The same configuration with the original work of DINO was adopted for comparison, with crop sizes of 0.4 - 1.0 and 0.05 - 0.4 for global and local views, respectively. Considering the relatively small dataset size and complexity of the medical image, we reduced the dimensionality of the DINO head output from 65,536 to 8,192.

For the foundation model learning with the proposed MS-DINO, Adam W optimizer (Loshchilov and Hutter, 2017) was used along with a cosine decay scheduler with a maximum learning rate of 0.00004 with a batch size of 8. The model was trained in the server-side device for 5 epochs. For training the foundation model with the DINO method via FL, the same optimizer, scheduler, and learning rate was used with a batch size of 4 per client, and the model was trained for 10,500 federated rounds in the client-side devices to match the total number of updates to MS-DINO learning in the server-side. For FL, both the student and teacher model parameters were averaged every 100 rounds.

For the downstream OAR segmentation task, the foundation ViT model and the UperNet (Xiao *et al.*, 2018) decoder were used as the encoder and the decoder, respectively, following the implementation in Bao *et al.* (2021); He *et al.* (2022). As the UNet for comparison, standard UNet (Ronneberger *et al.*, 2015) architecture with four downsample and upsample layers and 64 convolutional filters were utilized. We designed the decoder part of the network as the multi-class segmentation model, to delineate the ROIs (brainstem, optic chiasm, mandible, optic nerves, parotid glands, and submandibular glands) simultaneously. Following the previous work on MICCAI 2015 head and neck segmentation challenge dataset, we used the combined focal loss (Lin *et al.*, 2017) and Dice loss for the optimization. The SGD optimizer was used for the segmentation model with a learning rate of 0.01 and a batch size of 10.

For the downstream classification task, a simple linear layer was added as the classification head. As we implemented the tu-

erculosis diagnosis task as the binary classification, the model optimized with the BCE loss. Adam W optimizer was used to fine-tune the model for the classification task, with a learning rate of 0.0001 and a batch size of 16.

All experiments including data processing, foundation model learning, fine-tuning, and evaluation were performed with Python version 3.9 and Pytorch library 1.10 on NVIDIA GeForce RTX 3090, and the experiments on distributed learning were conducted with the FLOWER framework (Beutel *et al.*, 2020).

5.2. Details of evaluation

To evaluate the segmentation performance, the Dice similarity coefficient is used to quantify the overlap between the predicted segmentation mask and the ground truth label. To evaluate the classification performance, the area under the receiver operating characteristics curve (AUC) was calculated to compare the model performance, and the sensitivity, specificity, and accuracy were reported separately to provide detailed performances, after adjusting the thresholds to meet the pre-defined sensitivity value $\geq 80\%$, if possible.

5.3. Simulation for Feature Inversion Attack

We evaluated whether the permutation model is effective to prevent privacy attacks from feature hijacking, supposing the optimal configuration for the malicious attacker.

Following the previous work on the encryption with random patch permutation (Park and Ye, 2022), it is supposed that the attacker hijacked all encrypted features transmitted from all clients and knows the exact permutation ratio and patch size, the architecture of the unknown patch embedder and the dimensionality of position embedding. Specifically, the same architecture as the original patch embedder was used as the attacker-side feature embedder, and the three-layered discriminator and the four-layered generator from DCGAN (Radford *et al.*, 2015) were employed as the discriminator and decoder. As a jigsaw solver to solve the random permutation in the feature space, the transformer with 12 encoder layers and 12 attention heads was used. The discriminator was optimized with the modified version of GAN loss (Goodfellow *et al.*, 2014) as formulated in Eqs. (5) and (6), the combined $L1$ and $L2$ losses were used as the learning objective for the decoder, and the $L1$ loss was used as the objective for the jigsaw solver.

In addition, we supposed that the attacker possesses a sufficient amount of data in the same domain, like the CT or CXR available at the public repository, to train the attacker-side networks. As the attacker-side public data, 6,189 CT slices from the TCIA HNSCC-3DCT-RT data (Clark *et al.*, 2013; Bejarano *et al.*, 2018, 2019) and 9,577 normal CXRs data from the CheXpert data (Irvin *et al.*, 2019) were utilized.

The model was trained for 5 epochs with a batch size of 1 and a learning rate of 0.001.

6. Experimental results

6.1. Attention Changes with Foundation Model Training

Fig. 3 depict the changes in the last layer of multi-head attentions within the ViT model. Before the foundation model

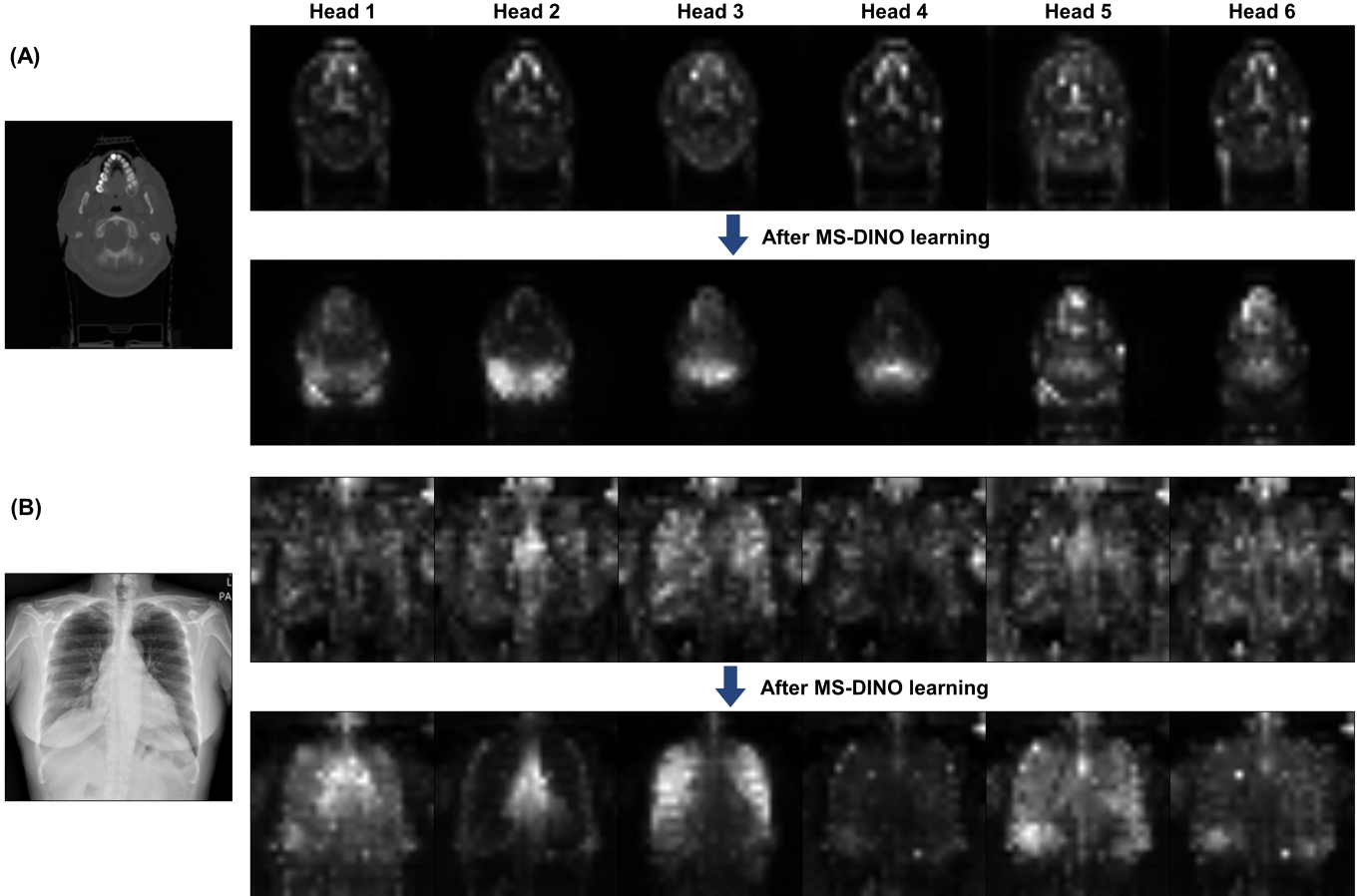


Fig. 3. Visualization of multi-head attention for (A) CT and (B) CXR. Compared with the attentions obtained with the pre-trained ImageNet weights, the different attention heads got refined and tend to concentrate on different semantic components after MS-DINO learning.

Table 3. Segmentation results after fine-tuning in data-limited setting

Method	Overall	Brainsetm	Chiasm	Mandible	Optic n Lt.	Optic n Rt.	Parotid Lt.	Parotid Rt.	SMG Lt.	SMG Rt.
Unet	0.083 (0.036)	0.182 (0.162)	0.000 (0.000)	0.359 (0.090)	0.000 (0.000)	0.000 (0.000)	0.067 (0.065)	0.134 (0.168)	0.002 (0.004)	0.000 (0.000)
ViT	0.437 (0.002)	0.628 (0.006)	0.085 (0.010)	0.602 (0.006)	0.213 (0.018)	0.060 (0.007)	0.623 (0.002)	0.607 (0.004)	0.538 (0.005)	0.577 (0.006)
ViT (DC DINO)	0.557 (0.003)	0.741 (0.024)	0.250 (0.020)	0.734 (0.011)	0.338 (0.016)	0.343 (0.010)	0.721 (0.006)	0.727 (0.021)	0.595 (0.008)	0.567 (0.042)
ViT (FL DINO)	0.538 (0.013)	0.732 (0.018)	0.202 (0.020)	0.716 (0.025)	0.327 (0.014)	0.286 (0.036)	0.689 (0.030)	0.716 (0.025)	0.567 (0.030)	<u>0.605</u> (0.035)
ViT (Proposed)	<u>0.556</u> <u>(0.010)</u>	<u>0.737</u> <u>(0.025)</u>	<u>0.232</u> <u>(0.006)</u>	0.740 (0.006)	<u>0.330</u> <u>(0.004)</u>	<u>0.320</u> <u>(0.030)</u>	0.725 (0.001)	<u>0.726</u> <u>(0.012)</u>	<u>0.589</u> <u>(0.043)</u>	0.606 (0.028)

Values are presented in the mean (standard deviation) of three repeats with different seeds.

DC DINO, data-centralized DINO; FL DINO, federated learning DINO

Bold face and underline denote the best and the second best performances.

training, the attentions of the ViT model with the ImageNet pre-trained with the original DINO disperse throughout the image (upper row), and the differences in attention between the individual heads were not prominent, implying that most attention heads process the image less effectively. After learning with the MS-DINO method, the different heads tend to attention to different semantic components (lower row), which can offer improved model performances with diverse patterns of self-attention.

6.2. Performance Comparison for Downstream CT Task

The comparison results for the CT task between the methods are provided in Table 3 and 4. The model fine-tuned from the foundation models showed better performance than those obtained with training from scratch. In particular, the model trained with the proposed MS-DINO showed a performance close to that of the DINO trained in a data-centralized manner, while outperforming the DINO trained with FL. The performance enhancement with the foundation model learning is

Table 4. Segmentation results after fine-tuning in data-abundant setting

Method	Overall	Brainsetm	Chiasm	Mandible	Optic n Lt.	Optic n Rt.	Parotid Lt.	Parotid Rt.	SMG Lt.	SMG Rt.
Unet	0.625 (0.014)	0.758 (0.013)	0.273 (0.012)	0.800 (0.007)	0.431 (0.029)	0.433 (0.072)	0.739 (0.013)	0.776 (0.004)	0.717 (0.002)	0.703 (0.024)
ViT	0.584 (0.002)	0.718 (0.002)	0.243 (0.007)	0.761 (0.004)	0.370 (0.000)	0.359 (0.012)	0.737 (0.003)	0.742 (0.002)	0.697 (0.004)	0.627 (0.012)
ViT (DC DINO)	0.658 (0.006)	0.764 (0.015)	0.320 (0.011)	<u>0.814</u> (0.013)	0.498 (0.003)	0.500 (0.004)	0.786 (0.004)	0.819 (0.002)	0.708 (0.031)	0.714 (0.005)
ViT (FL DINO)	0.653 (0.005)	0.775 (0.010)	0.278 (0.019)	0.810 (0.022)	0.485 (0.031)	0.443 (0.044)	0.778 (0.005)	0.814 (0.003)	0.730 (0.003)	0.706 (0.029)
ViT (Proposed)	<u>0.656</u> (0.002)	0.777 (0.014)	<u>0.313</u> (0.007)	0.818 (0.004)	<u>0.494</u> (0.014)	<u>0.460</u> (0.012)	<u>0.781</u> (0.006)	<u>0.817</u> (0.005)	0.740 (0.009)	0.699 (0.025)

Values are presented in the mean (standard deviation) of three repeats with different seeds.

DC DINO, data-centralized DINO; FL DINO, federated learning DINO

Bold face and underline denote the best and the second best performances.

Table 5. Classification results after fine-tuning in data-limited setting

Method	AUC	Sensitivity	Specificity	Accuracy
DenseNet-121	0.514 (0.006)	0.442 (0.066)	0.588 (0.089)	0.519 (0.042)
ViT	0.590 (0.004)	0.558 (0.013)	0.598 (0.011)	0.585 (0.004)
ViT (DC DINO)	<u>0.824</u> (0.016)	<u>0.739</u> (0.022)	<u>0.757</u> (0.045)	<u>0.751</u> (0.025)
ViT (FL DINO)	0.695 (0.057)	0.645 (0.066)	0.609 (0.058)	0.616 (0.029)
ViT (Proposed)	0.844 (0.007)	0.790 (0.063)	0.772 (0.011)	0.778 (0.022)

Values are presented in the mean (standard deviation) of three repeats with different seeds.

DC DINO, data-centralized DINO; FL DINO, federated learning DINO

Bold face and underline denote the best and the second best performances.

6.3. Performance comparison for downstream CXR task

Table 5 and 6 show the comparison results for the CXR task between the methods. Compared with the fine-tune-only baselines which were obtained by training the model from scratch, those with the foundation model offered generally better performance. Furthermore, among those with foundation models, the model trained with the proposed MS-DINO method provided the best performance, even outperforming the DINO trained in a data-centralized manner as well as the DINO obtained in FL. The benefit of the proposed method was remarkable in the data-limited setting, providing a diagnostic performance close to that of the data-abundant setting with only several hundred images for each class.

6.4. Communication costs

When defining the number of data as D , total training rounds as R , the round between aggregation and distribution as r , the model parameter as P , and the size of encrypted feature for each data as F , the total communication costs for foundation model learning T for the FL and the MS-DINO can be formulated as below:

$$T_{\text{FL}} = \frac{4R}{r} \times P, \quad (8)$$

$$T_{\text{MS-DINO}} = D \times F \quad (9)$$

where the constant 4 is multiplied to account for the parameter transmission of both the teacher and student models, and the both-way transmissions between server and client for FL. As the MS-DINO method does not require continuous communication between the server and the clients, the only communication between the server and clients occurs at the beginning of the learning.

With this formulation, the numerical comparison results are provided in Table 7. Compared to the training of DINO with FL, the communication cost of the proposed MS-DINO is about one-third, which can be further advantageous as the number of total rounds increases.

6.5. Experiments on Privacy protection

The qualitative and quantitative analysis results of reconstruction from the privacy attack are provided in Table 8 and Fig. 5.

more prominent in the data-limited than the data-abundant settings.

Fig. 4 depicts the qualitative comparison between methods. The model fine-tuned from the foundation model with the proposed MS-DINO offered overall more accurate predictions for the areas of OARs, which is comparable to those with data-centralized DINO and outperforms those of fine-tuning only baseline.

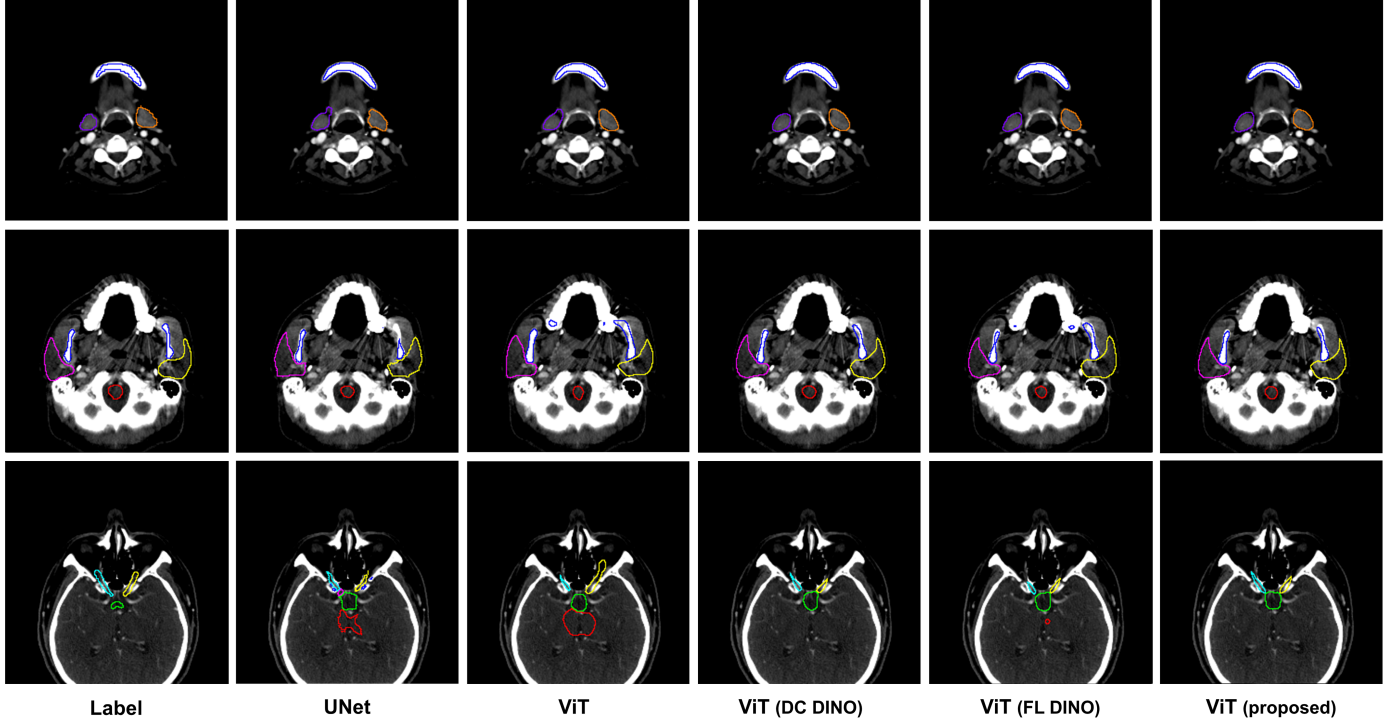


Fig. 4. Qualitative comparisons of the segmentation results. The model fine-tuned from the foundation model with the MS-DINO method shows results comparable to those with the data-centralized DINO method and outperforms the fine-tune only baselines. The results are obtained from fine-tuning in a data-abundant setting.

Table 7. Comparison of communication overheads between methods

Method	Continuous communication	Communication cost	
		Feature transmission	Model averaging
Federated learning	✓	-	12,229.7 M
Proposed	✗	4,866.9 M	-

Given the optimal configuration for the attacker and the setting that the *feature-space permutation module* is not employed, both the private CT and CXR data can be reconstructed to the amount that the privacy like shape, gender, anatomic location, and disease status of the subject can be inferred from the reconstruction results of hijacked feature to some degree. This implies that the approximate solution of the unknown feature embedder can be obtained by the attacker. However, when the extracted features are randomly permuted in the feature space, it was nearly impossible to reconstruct the data to the amount that the privacy can be inferred (Fig. 5).

Combined, these results confirm our claim that simultaneously solving two optimization problems that need each other's solution can be considered to be an underdetermined problem, and thus practically difficult to solve.

6.6. Ablation studies

Table 9 shows the ablation studies to verify the roles of the components of the proposed MS-DINO. As the random masked sampling and different augmentation for each image were utilized in the proposed method, we ablated the components in or-

der. The ablation studies are performed in the data-limited setting, as the benefit of the proposed method is more pronounced in this setting.

6.6.1. Random masked sampling

Ablating the random masked sampling means that the model is trained by the knowledge distillation between teacher and student, with the two views of the image, the original and the augmented versions of the same image, but without any random sub-sampling. As shown in the Table 9, the performances were suboptimal for both CT segmentation and CXR classification, implying that this component is indispensable for the best performance.

6.6.2. Augmentation

Next, we ablated the augmentation to offer two different views of the image to evaluate whether this component is necessary for performance. Compared with the proposed method leveraging an augmented version of the given image, applying random sampling solely for the original image show lower performance in both CT segmentation and CXR classification,

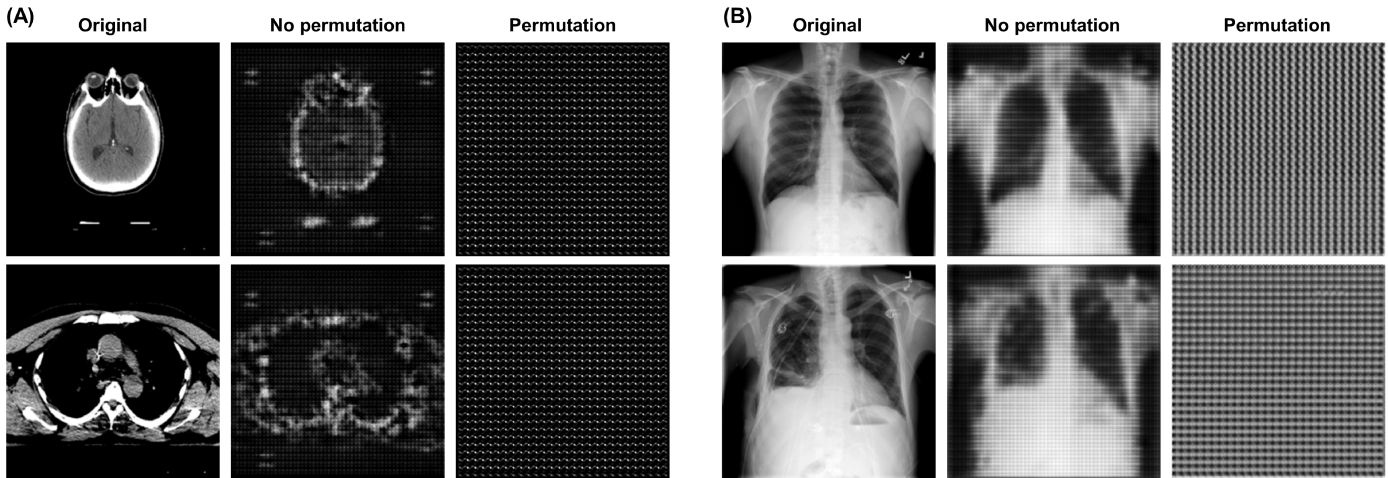


Fig. 5. Reconstruction results of the privacy attack for (A) CT and (B) CXR. Without the *feature-space permutation module*, information (level of CT slice, presence of disease, etc.) can be inferred from the reconstructed results, while it was infeasible when the *feature-space permutation module* was utilized.

Table 8. Quantitative comparison for privacy attack

Method	CT		CXR	
	MSE	SSIM	MSE	SSIM
No permutation	0.237 (0.005)	0.694 (0.008)	0.161 (0.051)	0.350 (0.014)
Permutation	0.272 (0.009)	0.479 (0.038)	0.267 (0.006)	0.018 (0.007)

Values are presented in the mean (standard deviation) of three repeats with different seeds.

MSE, mean squared error; SSIM, structural similarity index measure.

Table 9. Ablation studies

Method	CT Segmentation	CXR classification
	Overall DSC	AUC
Proposed	0.556 (0.010)	0.844 (0.007)
No random masking	0.544 (0.003)	0.817 (0.045)
No augmentation	0.548 (0.004)	0.833 (0.019)

Values are presented in the mean (standard deviation) of three repeats with different seeds.

OAR, organ at risk; DSC, dice similarity coefficient; AUC, area under the curve.

which suggests that offering different views of an image enhances the performance regardless of the modalities and the tasks.

7. Discussion and Conclusion

Despite surprising performance of the DL-based vision models, the data-driven learning paradigm of the DL has been posing practical hurdles in the development of the AI model for healthcare research where the data utilized for training may contain sensitive privacy of individuals (Perone and Cohen-Adad, 2019). In addition, the label dependency throws another challenge since the labels annotated by the medical experts are usually expensive and hard to be obtained (Willemink *et al.*, 2020).

Distributed learning methods have been introduced to tackle these problems by enabling model training without directly sharing private data, and self-supervised learning methods have been investigated to alleviate the label dependency of the DL

model. Several works have investigated the combination of these two techniques, but there remain problems in those approaches reporting suboptimal performances compared with data-centralized counterparts (Makhija *et al.*, 2022; Zhuang *et al.*, 2022; Shi *et al.*, 2021). Furthermore, the innate properties of model averaging during FL enforce continuous communication between server and clients for model averaging as well as high communication overhead, and pose the privacy threats that can be caused by the model inversion attack by malicious attackers (Geiping *et al.*, 2020; Lyu *et al.*, 2020b; Hatamizadeh *et al.*, 2022).

To alleviate these issues, we have introduced a novel self-supervised learning method, dubbed MS-DINO, that can be used in a distributed manner without continuous communication but still attains a performance comparable to or even outperforming the self-supervised learning method performed in a data-centralized setting. Inspired by the previous works that reported the intriguing properties of ViT (Naseer *et al.*, 2021; Park and Kim, 2022), we utilized two key concepts, the permutation-invariant property of the transformer layer and semantic learning via local-to-global correspondence using the teacher-student distillation, to devise our method. Specifically, we replaced the multi-crop strategy of cropping multiple small local crops and large global crops with the random masked sampling strategy, which randomly samples large and multiple small portions of the patch features. This random masking strategy is also consistent with pioneering self-supervised learning approaches that conjugate masked image modeling with the ViT models in a patch-wise manner (Bao *et al.*, 2021; He *et al.*, 2022; Xie *et al.*, 2022). Furthermore, we amalgamated the previously proposed *feature-space permutation module* (Park and Ye, 2022) to enhance privacy and to improve communication efficiency without defacing the performances. By enabling to save the encrypted patch features with the *feature-space permutation module*, the foundation model learning based on the masked random sampling of patch features can be performed solely on the server-side device while at the same time protect-

ing the privacy of the participating subjects. We performed extensive experiments on two imaging modalities and two tasks in both data-abundant and data-limited settings to clarify the benefit of the method in general application. In addition, we also performed experiments on the privacy attack to verify the efficacy of the *feature-space permutation module*, demonstrating that enhanced privacy can be offered with the proposed method equipped with this module.

Our study is not free of limitations. First, as the proposed MS-DINO method is built upon the intrinsic permutation-invariant property of the Transformer, the model without this property, for instance, CNN-based architecture, can not be utilized. Second, although we have demonstrated that the privacy attack through feature-space hijacking is infeasible for our method, other types of malicious attacks including model poisoning and data poisoning (Lyu *et al.*, 2020b; Tolpegin *et al.*, 2020; Bagdasaryan *et al.*, 2020) or privacy threats like the membership inference (Gupta *et al.*, 2021; Shokri *et al.*, 2017; Nasr *et al.*, 2019) were not investigated, which is beyond the scope of this work. The existing methods for privacy protection can be adopted in addition to the proposed method to enhance privacy (Lyu *et al.*, 2020a; Zhao *et al.*, 2019; Li *et al.*, 2020a). Third, other considerations for the practical implementation like the data skewness between clients were not investigated (Gao *et al.*, 2020). However, as the permuted features from all clients are saved and used by the server during the foundation model learning, the vulnerability to data skewness is expected to be lower compared with the existing approaches. Finally, our learning method is only applicable to the ViT-based models, since it is based on the model-specific learning method, the random masked sampling of the shuffled patch features. In addition, as the ViT model processes the image by dividing it into multiple patches and by calculating the attention scores, the fine-grained segmentation of the thin and small organ (e.g. optic chiasm) is difficult for the ViT-based model, as shown in the example in the third row of Fig. 4.

Nevertheless, given the limited data availability and the importance of privacy in health research, our method has great promise to build a general foundation model in a communication-efficient and privacy-protecting way. Since the model obtained with the proposed MS-DINO has a general understanding of visual semantics, it can be used as the task-agnostic foundation model to enhance the performances of the downstream task, suggesting its widespread applicability in healthcare research.

8. Acknowledgement

This research was supported in part by a grant of the MD-PhD/Medical Scientist Training Program through the Korea Health Industry Development Institute (KHIDI), funded by the Ministry of Health & Welfare, Republic of Korea, by the National Research Foundation of Korea (NRF) grant funded by the Korean Government Ministry of Science and ICT (NRF-2020R1A2C1102559), by a faculty research grant of Yonsei University College of Medicine (6-2019-0071), by the National Research Foundation of Korea under Grant NRF-

2020R1A2B5B03001980, and by the KAIST Key Research Institute (Interdisciplinary Research Group) Project.

Appendix A. Ethic Committee Approval

The CT and the ROI data collected for this study were ethically approved by the Institutional Review Board (IRB) of Gangnam Severance Hospital (IRB number: 3-2020-0289), and the requirement for informed consent was waived due to the retrospective nature of this study.

References

Bagdasaryan, E., Veit, A., Hua, Y., Estrin, D., Shmatikov, V., 2020. How to backdoor federated learning, in: International Conference on Artificial Intelligence and Statistics, PMLR, pp. 2938–2948.

Bao, H., Dong, L., Wei, F., 2021. Beit: Bert pre-training of image transformers. arXiv preprint arXiv:2106.08254.

Bejarano, T., De Ornelas Couto, M., Mihaylov, I.B., 2018. Head-and-neck squamous cell carcinoma patients with ct taken during pre-treatment, mid-treatment, and post-treatment dataset. The Cancer Imaging Archive 10, K9.

Bejarano, T., De Ornelas-Couto, M., Mihaylov, I.B., 2019. Longitudinal fan-beam computed tomography dataset for head-and-neck squamous cell carcinoma patients. Medical physics 46, 2526–2537.

Beutel, D.J., Topal, T., Mathur, A., Qiu, X., Parcollet, T., de Gusmão, P.P., Lane, N.D., 2020. Flower: A friendly federated learning research framework. arXiv preprint arXiv:2007.14390.

Caron, M., Touvron, H., Misra, I., Jégou, H., Mairal, J., Bojanowski, P., Joulin, A., 2021. Emerging properties in self-supervised vision transformers. arXiv preprint arXiv:2104.14294.

Chen, M., Radford, A., Child, R., Wu, J., Jun, H., Luan, D., Sutskever, I., 2020a. Generative pretraining from pixels, in: International conference on machine learning, PMLR, pp. 1691–1703.

Chen, T., Kornblith, S., Norouzi, M., Hinton, G., 2020b. A simple framework for contrastive learning of visual representations, in: International conference on machine learning, PMLR, pp. 1597–1607.

Clark, K., Vendt, B., Smith, K., Freymann, J., Kirby, J., Koppel, P., Moore, S., Phillips, S., Maffitt, D., Pringle, M., *et al.*, 2013. The cancer imaging archive (tcia): maintaining and operating a public information repository. Journal of digital imaging 26, 1045–1057.

Computing, M.I., Interventions, C.A., 2015. Head and neck auto segmentation miccai challenge. <https://www.imagenglab.com/newsite/pddca/>. (Accessed on 11/16/2022).

Devlin, J., Chang, M.W., Lee, K., Toutanova, K., 2018. Bert: Pre-training of deep bidirectional transformers for language understanding. arXiv preprint arXiv:1810.04805.

Dosovitskiy, A., Beyer, L., Kolesnikov, A., Weissenborn, D., Zhai, X., Unterthiner, T., Dehghani, M., Minderer, M., Heigold, G., Gelly, S., *et al.*, 2020. An image is worth 16x16 words: Transformers for image recognition at scale. arXiv preprint arXiv:2010.11929.

Edemekong, P.F., Annamaraju, P., Haydel, M.J., 2018. Health insurance portability and accountability act.

Elhalawani, H., Mohamed, A.S., White, A.L., Zafereo, J., Wong, A.J., Berends, J.E., AboHashem, S., Williams, B., Aymard, J.M., Kanwar, A., *et al.*, 2017. Matched computed tomography segmentation and demographic data for oropharyngeal cancer radiomics challenges. Scientific data 4, 170077.

Gao, Y., Kim, M., Abuadba, S., Kim, Y., Thapa, C., Kim, K., Camtepe, S.A., Kim, H., Nepal, S., 2020. End-to-end evaluation of federated learning and split learning for internet of things. arXiv preprint arXiv:2003.13376.

Gawron, G., Stubbings, P., 2022. Feature space hijacking attacks against differentially private split learning. arXiv preprint arXiv:2201.04018.

Geiping, J., Bauermeister, H., Dröge, H., Moeller, M., 2020. Inverting gradients-how easy is it to break privacy in federated learning? Advances in Neural Information Processing Systems 33, 16937–16947.

Giger, M.L., 2018. Machine learning in medical imaging. Journal of the American College of Radiology 15, 512–520.

Goodfellow, I., Pouget-Abadie, J., Mirza, M., Xu, B., Warde-Farley, D., Ozair, S., Courville, A., Bengio, Y., 2014. Generative adversarial nets. Advances in neural information processing systems 27.

Grill, J.B., Strub, F., Alché, F., Tallec, C., Richemond, P., Buchatskaya, E., Doersch, C., Avila Pires, B., Guo, Z., Gheshlaghi Azar, M., et al., 2020. Bootstrap your own latent-a new approach to self-supervised learning. *Advances in neural information processing systems* 33, 21271–21284.

Grossberg, A.J., Mohamed, A.S., Elhalawani, H., Bennett, W.C., Smith, K.E., Nolan, T.S., Williams, B., Chamchod, S., Heukelom, J., Kantor, M.E., et al., 2018. Imaging and clinical data archive for head and neck squamous cell carcinoma patients treated with radiotherapy. *Scientific data* 5, 1–10.

Grossberg, A.E.H., Mohamed, A.M.S., Williams, B.W.A., Zafereo, J.W.A., Berends, J.E.A.S., Aymard, J.M., K.A., Perni, S.R.C., Chamchod, S.K.M., Browne, T.H.K., Gunn, G.B., F.S., Rosenthal, D.I., G.A., CD, F., 2020. Hnsc [dataset]. M.D. Anderson Cancer Center Head and Neck Quantitative Imaging Working Group.

Gupta, U., Stripelis, D., Lam, P.K., Thompson, P., Ambite, J.L., Ver Steeg, G., 2021. Membership inference attacks on deep regression models for neuroimaging, in: *Medical Imaging with Deep Learning*, PMLR. pp. 228–251.

Hatamizadeh, A., Yin, H., Molchanov, P., Myronenko, A., Li, W., Dogra, P., Feng, A., Flores, M.G., Kautz, J., Xu, D., et al., 2022. Do gradient inversion attacks make federated learning unsafe? *arXiv preprint arXiv:2202.06924*.

He, K., Chen, X., Xie, S., Li, Y., Dollár, P., Girshick, R., 2022. Masked autoencoders are scalable vision learners, in: *Proceedings of the IEEE/CVF Conference on Computer Vision and Pattern Recognition*, pp. 16000–16009.

Hoofnagle, C.J., van der Sloot, B., Borgesius, F.Z., 2019. The european union general data protection regulation: what it is and what it means. *Information & Communications Technology Law* 28, 65–98.

Irvin, J., Rajpurkar, P., Ko, M., Yu, Y., Ciurea-Ilcus, S., Chute, C., Marklund, H., Haghgoor, B., Ball, R., Shpanskaya, K., et al., 2019. CheXpert: A large chest radiograph dataset with uncertainty labels and expert comparison, in: *Proceedings of the AAAI conference on artificial intelligence*, pp. 590–597.

Jaeger, S., Candemir, S., Antani, S., Wáng, Y.X.J., Lu, P.X., Thoma, G., 2014. Two public chest x-ray datasets for computer-aided screening of pulmonary diseases. *Quantitative imaging in medicine and surgery* 4, 475.

Jaiswal, A., Babu, A.R., Zadeh, M.Z., Banerjee, D., Makedon, F., 2020. A survey on contrastive self-supervised learning. *Technologies* 9, 2.

Jing, L., Tian, Y., 2020. Self-supervised visual feature learning with deep neural networks: A survey. *IEEE transactions on pattern analysis and machine intelligence* 43, 4037–4058.

Konečný, J., McMahan, H.B., Yu, F.X., Richtárik, P., Suresh, A.T., Bacon, D., 2016. Federated learning: Strategies for improving communication efficiency. *arXiv preprint arXiv:1610.05492*.

Lee, J.G., Jun, S., Cho, Y.W., Lee, H., Kim, G.B., Seo, J.B., Kim, N., 2017. Deep learning in medical imaging: general overview. *Korean journal of radiology* 18, 570–584.

Li, S., Cheng, Y., Wang, W., Liu, Y., Chen, T., 2020a. Learning to detect malicious clients for robust federated learning. *arXiv preprint arXiv:2002.00211*.

Li, T., Sahu, A.K., Talwalkar, A., Smith, V., 2020b. Federated learning: Challenges, methods, and future directions. *IEEE Signal Processing Magazine* 37, 50–60.

Lin, T.Y., Goyal, P., Girshick, R., He, K., Dollár, P., 2017. Focal loss for dense object detection, in: *Proceedings of the IEEE international conference on computer vision*, pp. 2980–2988.

Liu, X., Zhang, F., Hou, Z., Mian, L., Wang, Z., Zhang, J., Tang, J., 2021. Self-supervised learning: Generative or contrastive. *IEEE Transactions on Knowledge and Data Engineering*.

Liu, Y., Wu, Y.H., Ban, Y., Wang, H., Cheng, M.M., 2020. Rethinking computer-aided tuberculosis diagnosis, in: *Proceedings of the IEEE/CVF Conference on Computer Vision and Pattern Recognition*, pp. 2646–2655.

Loshchilov, I., Hutter, F., 2017. Decoupled weight decay regularization. *arXiv preprint arXiv:1711.05101*.

Lyu, L., Yu, H., Ma, X., Sun, L., Zhao, J., Yang, Q., Yu, P.S., 2020a. Privacy and robustness in federated learning: Attacks and defenses. *arXiv preprint arXiv:2012.06337*.

Lyu, L., Yu, H., Yang, Q., 2020b. Threats to federated learning: A survey. *arXiv preprint arXiv:2003.02133*.

Makhija, D., Ho, N., Ghosh, J., 2022. Federated self-supervised learning for heterogeneous clients. *arXiv preprint arXiv:2205.12493*.

Mammen, P.M., 2021. Federated learning: Opportunities and challenges. *arXiv preprint arXiv:2101.05428*.

Naseer, M.M., Ranasinghe, K., Khan, S.H., Hayat, M., Shahbaz Khan, F., Yang, M.H., 2021. Intriguing properties of vision transformers. *Advances in Neural Information Processing Systems* 34, 23296–23308.

Nasr, M., Shokri, R., Houmansadr, A., 2019. Comprehensive privacy analysis of deep learning: Passive and active white-box inference attacks against centralized and federated learning, in: *2019 IEEE symposium on security and privacy (SP)*, IEEE. pp. 739–753.

of North America, R.S., 2018. Rnna pneumonia detection challenge. <https://www.kaggle.com/c/rsna-pneumonia-detection-challenge>. (Accessed on 11/16/2022).

Park, N., Kim, S., 2022. How do vision transformers work? *arXiv preprint arXiv:2202.06709*.

Park, S., Kim, G., Kim, J., Kim, B., Ye, J.C., 2021. Federated split task-agnostic vision transformer for covid-19 cxr diagnosis. *Advances in Neural Information Processing Systems* 34, 24617–24630.

Park, S., Ye, J.C., 2022. Multi-task distributed learning using vision transformer with random patch permutation. *IEEE Transactions on Medical Imaging* , 1–1doi:10.1109/TMI.2022.3218783.

Perone, C.S., Cohen-Adad, J., 2019. Promises and limitations of deep learning for medical image segmentation. *J Med Artif Intell* 2, 1–2.

Pesapane, F., Codari, M., Sardanelli, F., 2018. Artificial intelligence in medical imaging: threat or opportunity? radiologists again at the forefront of innovation in medicine. *European radiology experimental* 2, 1–10.

radder, . Tbxpredict - browse /data at sourceforge.net. <https://www.kaggle.com/raddrad/chest-xrays-tuberculosis-from-india>. (Accessed on 11/22/2022).

Radford, A., Metz, L., Chintala, S., 2015. Unsupervised representation learning with deep convolutional generative adversarial networks. *arXiv preprint arXiv:1511.06434*.

Ronneberger, O., Fischer, P., Brox, T., 2015. U-net: Convolutional networks for biomedical image segmentation, in: *International Conference on Medical image computing and computer-assisted intervention*, Springer. pp. 234–241.

Shi, H., Zhang, Y., Shen, Z., Tang, S., Li, Y., Guo, Y., Zhuang, Y., 2021. Towards communication-efficient and privacy-preserving federated representation learning. *arXiv preprint arXiv:2109.14611*.

Shokri, R., Stronati, M., Song, C., Shmatikov, V., 2017. Membership inference attacks against machine learning models, in: *2017 IEEE symposium on security and privacy (SP)*, IEEE. pp. 3–18.

Ting, D.S., Liu, Y., Burlina, P., Xu, X., Bressler, N.M., Wong, T.Y., 2018. Ai for medical imaging goes deep. *Nature medicine* 24, 539–540.

Tolpegin, V., Truex, S., Gursoy, M.E., Liu, L., 2020. Data poisoning attacks against federated learning systems, in: *European Symposium on Research in Computer Security*, Springer. pp. 480–501.

Vepakomma, P., Gupta, O., Swedish, T., Raskar, R., 2018. Split learning for health: Distributed deep learning without sharing raw patient data. *arXiv preprint arXiv:1812.00564*.

Willemink, M.J., Koszek, W.A., Hardell, C., Wu, J., Fleischmann, D., Harvey, H., Folio, L.R., Summers, R.M., Rubin, D.L., Lungren, M.P., 2020. Preparing medical imaging data for machine learning. *Radiology* 295, 4–15.

Xiao, T., Liu, Y., Zhou, B., Jiang, Y., Sun, J., 2018. Unified perceptual parsing for scene understanding, in: *Proceedings of the European conference on computer vision (ECCV)*, pp. 418–434.

Xie, Z., Zhang, Z., Cao, Y., Lin, Y., Bao, J., Yao, Z., Dai, Q., Hu, H., 2022. Simmim: A simple framework for masked image modeling, in: *Proceedings of the IEEE/CVF Conference on Computer Vision and Pattern Recognition*, pp. 9653–9663.

Zbontar, J., Jing, L., Misra, I., LeCun, Y., Deny, S., 2021. Barlow twins: Self-supervised learning via redundancy reduction, in: *International Conference on Machine Learning*, PMLR. pp. 12310–12320.

Zhao, Y., Chen, J., Zhang, J., Wu, D., Teng, J., Yu, S., 2019. Pdgan: A novel poisoning defense method in federated learning using generative adversarial network, in: *International Conference on Algorithms and Architectures for Parallel Processing*, Springer. pp. 595–609.

Zhuang, W., Wen, Y., Zhang, S., 2022. Divergence-aware federated self-supervised learning. *arXiv preprint arXiv:2204.04385*.